

Combined CDF and DØ Upper Limits on Standard Model Higgs-Boson Production with up to 4.2 fb^{-1} of Data

The TEVNPH Working Group*
for the CDF and DØ Collaborations

August 14, 2019

We combine results from CDF and DØ on direct searches for a standard model (SM) Higgs boson (H) in $p\bar{p}$ collisions at the Fermilab Tevatron at $\sqrt{s} = 1.96 \text{ TeV}$. Compared to the previous Higgs Tevatron combination, more data and new channels ($WH \rightarrow \tau\nu b\bar{b}$, $VH \rightarrow \tau\tau b\bar{b}/jj\tau\tau$, $VH \rightarrow jjb\bar{b}$, $t\bar{t}H \rightarrow t\bar{t}b\bar{b}$) have been added. Most previously used channels have been reanalyzed to gain sensitivity. We use the latest parton distribution functions and $gg \rightarrow H$ theoretical cross sections when comparing our limits to the SM predictions. With $2.0\text{-}3.6 \text{ fb}^{-1}$ of data analyzed at CDF, and $0.9\text{-}4.2 \text{ fb}^{-1}$ at DØ, the 95% C.L. upper limits on Higgs boson production are a factor of 2.5 (0.86) times the SM cross section for a Higgs boson mass of $m_H = 115$ (165) GeV/c^2 . Based on simulation, the corresponding median expected upper limits are 2.4 (1.1). The mass range excluded at 95% C.L. for a SM Higgs has been extended to $160 < m_H < 170 \text{ GeV}/c^2$.

Preliminary Results

* The Tevatron New-Phenomena and Higgs working group can be contacted at TEVNPHWG@fnal.gov. More information can be found at <http://tevnphwg.fnal.gov/>.

I. INTRODUCTION

The search for a mechanism for electroweak symmetry breaking, and in particular for a standard model (SM) Higgs boson has been a major goal of particle physics for many years, and is a central part of the Fermilab Tevatron physics program. Both the CDF and DØ experiments are reporting new combinations [1, 2] of multiple direct searches for the SM Higgs boson. The new searches include more data and improved analysis techniques compared to previous analyses. The sensitivities of these new combinations significantly exceed previous work [3, 4]. The most recent Tevatron Higgs combination [5] only included channels seeking Higgs bosons of masses between 155 and 200 GeV/ c^2 , and the most recent combination over the entire mass range 100-200 GeV/ c^2 was reported in April 2008 [6].

In this note, we combine the most recent results of all such searches in $p\bar{p}$ collisions at $\sqrt{s} = 1.96$ TeV. The analyses combined here seek signals of Higgs bosons produced in association with vector bosons ($q\bar{q} \rightarrow W/ZH$), through gluon-gluon fusion ($gg \rightarrow H$), and through vector boson fusion (VBF) ($q\bar{q} \rightarrow q'\bar{q}'H$) corresponding to integrated luminosities ranging from 2.0-3.6 fb $^{-1}$ at CDF and 0.9-4.2 fb $^{-1}$ at DØ. The Higgs boson decay modes studied are $H \rightarrow b\bar{b}$, $H \rightarrow W^+W^-$, $H \rightarrow \tau^+\tau^-$ and $H \rightarrow \gamma\gamma$.

To simplify the combination, the searches are separated into 75 mutually exclusive final states (23 for CDF and 52 for DØ; see Table I and II) referred to as “analyses” in this note. The selection procedures for each analysis are detailed in Refs. [7] through [20], and are briefly described below.

II. ACCEPTANCE, BACKGROUNDS AND LUMINOSITY

Event selections are similar for the corresponding CDF and DØ analyses. For the case of $WH \rightarrow \ell\nu b\bar{b}$, an isolated lepton ($\ell =$ electron or muon) and two jets are required, with one or more b -tagged jet, i.e., identified as containing a weakly-decaying B hadron. Selected events must also display a significant imbalance in transverse momentum (referred to as missing transverse energy or \cancel{E}_T). Events with more than one isolated lepton are vetoed. For the DØ $WH \rightarrow \ell\nu b\bar{b}$ analyses, two and three jet events are analyzed separately, and in each of these samples two non-overlapping b -tagged samples are defined, one being a single “tight” b -tag (ST) sample, and the other a double “loose” b -tag (DT) sample. The tight and loose b -tagging criteria are defined with respect to the mis-identification rate that the b -tagging algorithm yields for light quark or gluon jets (“mistag rate”) typically $\leq 0.5\%$ or $\leq 1.5\%$, respectively. The final variable is a neural network output which takes as input seven kinematics variables and a matrix element discriminant for the 2 jet sample, while for the 3 jet sample the dijet invariant mass is used. In this combination, we add a new analysis $WH \rightarrow \tau\nu b\bar{b}$ in which the τ is identified through its hadronic decays. This analysis is sensitive to $ZH \rightarrow \tau\cancel{E}_T b\bar{b}$ as well in those cases where a τ fails to be identified. The analysis is carried out according to the type of reconstructed τ and is also separated into two and three jets with DT events only. It uses the dijet invariant mass of the $b\bar{b}$ system as discriminant variable.

For the CDF $WH \rightarrow \ell\nu b\bar{b}$ analyses, the events are grouped into six categories. In addition to the selections requiring an identified lepton, events with an isolated track failing lepton selection requirements are grouped into their own categories. This provides some acceptance for single prong tau decays. Within the lepton categories there are three b -tagging categories – two tight b -tags (TDT), one tight b -tag and one loose b -tag (LDT), and a single, tight, b -tag (ST). In each category, two discriminants are calculated for each event. One neural network discriminant is trained at each m_H in the test range, separately for each category. A second discriminant is a boosted decision tree, featuring not only event kinematic and b -tagging observables, but matrix element discriminants as well. These two discriminants are then combined together using an evolutionary neural network [21] to form a single discriminant with optimal performance.

For the $ZH \rightarrow \nu\bar{\nu} b\bar{b}$ analyses, the selection is similar to the WH selection, except all events with isolated leptons are vetoed and stronger multijet background suppression techniques are applied. Both CDF and DØ analyses use a track-based missing transverse momentum calculation as a discriminant against false \cancel{E}_T . There is a sizable fraction of $WH \rightarrow \ell\nu b\bar{b}$ signal in which the lepton is undetected, that is selected in the $ZH \rightarrow \nu\bar{\nu} b\bar{b}$ samples, so these analyses are also referred to as $VH \rightarrow \cancel{E}_T b\bar{b}$. The CDF analysis uses three non-overlapping samples of events (TDT, LDT and ST as for WH) while DØ uses a sample of events having one tight b -tag jet and one loose b -tag jet. CDF used neural-network discriminants as the final variables, while DØ uses boosted decision trees as advanced analysis

technique.

The $ZH \rightarrow \ell^+ \ell^- b \bar{b}$ analyses require two isolated leptons and at least two jets. They use non-overlapping samples of events with one tight b -tag and two loose b -tags. For the $D\mathcal{O}$ analysis neural-network and boosted decision trees discriminants are the final variables for setting limits (depending on the sub-channel), while CDF uses the output of a 2-dimensional neural-network. CDF corrects jet energies for \cancel{E}_T using a neural network approach. In this analysis also the events are divided into three tagging categories: tight double tags, loose double tags, and single tags.

For the $H \rightarrow W^+ W^-$ analyses, signal events are characterized by a large \cancel{E}_T and two opposite-signed, isolated leptons. The presence of neutrinos in the final state prevents the reconstruction of the candidate Higgs boson mass. $D\mathcal{O}$ selects events containing electrons and muons, dividing the data sample into three final states: $e^+ e^-$, $e^\pm \mu^\mp$, and $\mu^+ \mu^-$. CDF separates the $H \rightarrow W^+ W^-$ events in five non-overlapping samples, labeled “high s/b ” and “low s/b ” for the lepton selection categories, and also split by the number of jets: 0, 1, or 2+ jets. The sample with two or more jets is not split into low s/b and high s/b lepton categories. The division of events into jet categories allows the analysis discriminants to separate three different categories of signals from the backgrounds more effectively. The signal production mechanisms considered are $gg \rightarrow H \rightarrow W^+ W^-$, $WH + ZH \rightarrow jjW^+ W^-$, and the vector-boson fusion process. The final discriminants are neural-network outputs for $D\mathcal{O}$ and neural-network output including likelihoods constructed from matrix-element probabilities (ME) as input to the neural network, for CDF, in the 0-jet bin, else the ME are not used. All analyses in this channel have been updated with more data and analysis improvements.

The CDF collaboration also contributes an analysis searching for Higgs bosons decaying to a tau lepton pair, in three separate production channels: direct $p\bar{p} \rightarrow H$ production, associated WH or ZH production, or vector boson production with H and forward jets in the final state. In this analysis, the final variable for setting limits is a combination of several neural-network discriminants.

$D\mathcal{O}$ also contributes a new analysis for the final state $\tau\tau$ jet jet, which is sensitive to the $VH \rightarrow jj\tau\tau$, $ZH \rightarrow \tau\tau b\bar{b}$, VBF and gluon gluon fusion (with two additional jets) mechanisms. It uses a neural network output as discriminant variable.

The CDF collaboration introduces a new all-hadronic channel, $WH + ZH \rightarrow jjb\bar{b}$ for this combination. Events are selected with four jets, at least two of which are b -tagged with the tight b -tagger. The large QCD backgrounds are estimated with the use of data control samples, and the final variable is a matrix element signal probability discriminant.

The $D\mathcal{O}$ collaboration contributes three $WH \rightarrow WW^+ W^-$ analyses, where the associated W boson and the W boson from the Higgs boson decay which has the same charge are required to decay leptonically, thereby defining three like-sign dilepton final states ($e^\pm e^\pm$, $e^\pm \mu^\pm$, and $\mu^\pm \mu^\pm$) containing all decays of the third W boson. In this analysis, which has not been updated for this combination, the final variable is a likelihood discriminant formed from several topological variables. CDF contributes a $WH \rightarrow WW^+ W^-$ analysis using a selection of like-sign dileptons and a neural network to further purify the signal. $D\mathcal{O}$ also contributes an analysis searching for direct Higgs boson production decaying to a photon pair in 4.2 fb^{-1} of data. In this analysis, the final variable is the invariant mass of the two-photon system.

Another new search from $D\mathcal{O}$ is included in this combination, namely the search for $t\bar{t}H \rightarrow t\bar{t}b\bar{b}$. Here the samples are analyzed independently according to the number of b -tagged jets (1,2,3, i.e. ST,DT,TT) and the total number of jets (4 or 5). The total transverse energy of the reconstructed objects (H_T) is used as discriminant variable.

All Higgs boson signals are simulated using PYTHIA [22], and CTEQ5L or CTEQ6L [23] leading-order (LO) parton distribution functions. The $gg \rightarrow H$ production cross section is calculated at NNLL in QCD and also includes two-loop electroweak effects; see Refs. [24, 25] and references therein for the different steps of these calculations. The newer calculation includes a more thorough treatment of higher-order radiative corrections, particularly those involving b quark loops. The $gg \rightarrow H$ production cross section depends strongly on the PDF set chosen and the accompanying value of α_s . The cross sections used here are calculated with the MSTW 2008 NNLO PDF set [29]. The new $gg \rightarrow H$ cross sections supersede those used in the update of Summer 2008 [5, 26, 28], which had a simpler treatment of radiative corrections and used the older MRST 2002 PDF set [30]. The Higgs boson production cross sections used here are listed in Table III [25]. We include all significant Higgs production modes in the high mass search: besides gluon-gluon fusion through a virtual top quark loop (ggH), we include production in association with a W or Z vector boson (VH) [27, 31, 32], and vector boson fusion (VBF) [27, 33].

The Higgs boson decay branching ratio predictions are calculated with HDECAY [34]. For both CDF and $D\mathcal{O}$, events from multijet (instrumental) backgrounds (“QCD production”) are measured in data with different methods, in

orthogonal samples. For CDF, backgrounds from other SM processes were generated using PYTHIA, ALPGEN [35], MC@NLO [36] and HERWIG [37] programs. For $D\bar{O}$, these backgrounds were generated using PYTHIA, ALPGEN, and COMPHEP [38], with PYTHIA providing parton-showering and hadronization for all the generators. These background processes were normalized using either experimental data or next-to-leading order calculations (from MCFM [39] for W + heavy flavor process).

Integrated luminosities, and references to the collaborations' public documentation for each analysis are given in Table I for CDF and in Table II for $D\bar{O}$. The tables include the ranges of Higgs boson mass (m_H) over which the searches were performed.

TABLE I: Luminosity, explored mass range and references for the different processes and final state ($\ell = e, \mu$) for the CDF analyses

Channel	Luminosity (fb^{-1})	m_H range (GeV/c^2)	Reference
$WH \rightarrow \ell\nu b\bar{b}$ $2\times(\text{TDT,LDT,ST})$	2.7	100-150	[7]
$ZH \rightarrow \nu\bar{\nu} b\bar{b}$ (TDT,LDT,ST)	2.1	105-150	[8]
$ZH \rightarrow \ell^+\ell^- b\bar{b}$ $2\times(\text{TDT,LDT,ST})$	2.7	100-150	[9]
$H \rightarrow W^+W^-$ (low,high s/b) $\times(0,1 \text{ jets})+(2+ \text{ jets})$	3.6	110-200	[10]
$WH \rightarrow WW^+W^- \rightarrow \ell^\pm\nu\ell^\pm\nu$	3.6	110-200	[10]
$H + X \rightarrow \tau^+\tau^- + 2 \text{ jets}$	2.0	110-150	[11]
$WH + ZH \rightarrow jjb\bar{b}$	2.0	100-150	[12]

TABLE II: Luminosity, explored mass range and references for the different processes and final state ($\ell = e, \mu$) for the $D\bar{O}$ analyses

Channel	Luminosity (fb^{-1})	m_H range (GeV/c^2)	Reference
$WH \rightarrow \ell\nu b\bar{b}$ $2\times(\text{ST,DT})$	2.7	100-150	[13]
$WH \rightarrow \tau\nu b\bar{b}$ $2\times(\text{ST,DT})$	0.9	105-145	[14]
$VH \rightarrow \tau\tau b\bar{b}/q\bar{q}\tau\tau$	1.0	105-145	[14]
$ZH \rightarrow \nu\bar{\nu} b\bar{b}$ (DT)	2.1	105-145	[15]
$ZH \rightarrow \ell^+\ell^- b\bar{b}$ $2\times(\text{ST,DT})$	2.3	105-145	[16]
$WH \rightarrow WW^+W^- \rightarrow \ell^\pm\nu\ell^\pm\nu$	1.1	120-200	[17]
$H \rightarrow W^+W^- \rightarrow \ell^\pm\nu\ell^\mp\nu$	3.0-4.2	115-200	[18]
$H \rightarrow \gamma\gamma$	4.2	100-150	[19]
$t\bar{t}H \rightarrow t\bar{t}b\bar{b}$ $2\times(\text{ST,DT,TT})$	2.1	105-145	[20]

III. DISTRIBUTIONS OF CANDIDATES

The number of channels combined is quite large, and the number of bins in each channel is large. Therefore, the task of assembling histograms and checking whether the expected and observed limits are consistent with the input predictions and observed data is difficult. We therefore provide histograms that aggregate all channels' signal, background, and data together. In order to preserve most of the sensitivity gain that is achieved by the analyses by binning the data instead of collecting them all together and counting, we aggregate the data and predictions in narrow bins of signal-to-background ratio, s/b . Data with similar s/b may be added together with no loss in sensitivity, assuming similar systematic errors on the predictions. The aggregate histograms do not show the effects of systematic uncertainties, but instead compare the data with the central predictions supplied by each analysis.

TABLE III: The (N)NLO production cross sections and decay branching fractions for the SM Higgs boson assumed for the combination

m_H (GeV/ c^2)	$\sigma_{gg \rightarrow H}$ (fb)	σ_{WH} (fb)	σ_{ZH} (fb)	σ_{VBF} (fb)	$B(H \rightarrow b\bar{b})$ (%)	$B(H \rightarrow \tau^+\tau^-)$ (%)	$B(H \rightarrow W^+W^-)$ (%)
100	1861	286.1	166.7	99.5	81.21	7.924	1.009
105	1618	244.6	144.0	93.3	79.57	7.838	2.216
110	1413	209.2	124.3	87.1	77.02	7.656	4.411
115	1240	178.8	107.4	79.07	73.22	7.340	7.974
120	1093	152.9	92.7	71.65	67.89	6.861	13.20
125	967	132.4	81.1	67.37	60.97	6.210	20.18
130	858	114.7	70.9	62.5	52.71	5.408	28.69
135	764	99.3	62.0	57.65	43.62	4.507	38.28
140	682	86.0	54.2	52.59	34.36	3.574	48.33
145	611	75.3	48.0	49.15	25.56	2.676	58.33
150	548	66.0	42.5	45.67	17.57	1.851	68.17
155	492	57.8	37.6	42.19	10.49	1.112	78.23
160	439	50.7	33.3	38.59	4.00	0.426	90.11
165	389	44.4	29.5	36.09	1.265	0.136	96.10
170	349	38.9	26.1	33.58	0.846	0.091	96.53
175	314	34.6	23.3	31.11	0.663	0.072	95.94
180	283	30.7	20.8	28.57	0.541	0.059	93.45
185	255	27.3	18.6	26.81	0.420	0.046	83.79
190	231	24.3	16.6	24.88	0.342	0.038	77.61
195	210	21.7	15.0	23	0.295	0.033	74.95
200	192	19.3	13.5	21.19	0.260	0.029	73.47

The range of s/b is quite large in each analysis, and so $\log_{10}(s/b)$ is chosen as the plotting variable. Plots of the distributions of $\log_{10}(s/b)$ are shown for $m_H = 115$ and 165 GeV/ c^2 in Figure 1. These distributions can be integrated from the high- s/b side downwards, showing the sums of signal, background, and data for the most pure portions of the selection of all channels added together. These integrals can be seen in Figure 2.

IV. COMBINING CHANNELS

To gain confidence that the final result does not depend on the details of the statistical formulation, we perform two types of combinations, using the Bayesian and Modified Frequentist approaches, which give similar results (within 10%). Both methods rely on distributions in the final discriminants, and not just on their single integrated values. Systematic uncertainties enter as uncertainties on the expected number of signal and background events, as well as on the distribution of the discriminants in each analysis (“shape uncertainties”). Both methods use likelihood calculations based on Poisson probabilities.

A. Bayesian Method

Because there is no experimental information on the production cross section for the Higgs boson, in the Bayesian technique [1] we assign a flat prior for the total number of selected Higgs events. For a given Higgs boson mass, the combined likelihood is a product of likelihoods for the individual channels, each of which is a product over histogram bins:

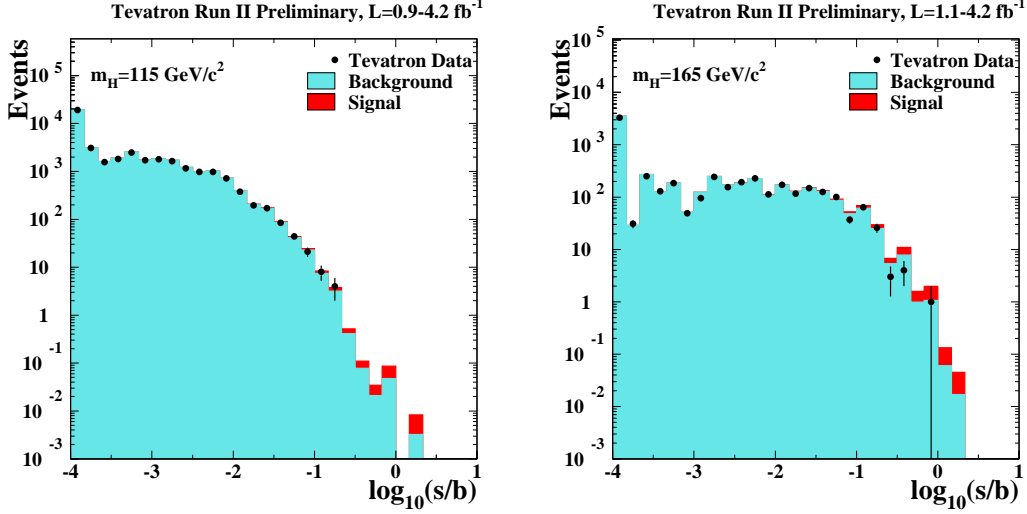


FIG. 1: Distributions of $\log_{10}(s/b)$, for the data from all contributing channels from CDF and DØ, for Higgs boson masses of 115 and 165 GeV/c^2 . The data are shown with points, and the signal is shown stacked on top of the backgrounds. Underflows and overflows are collected into the bottom and top bins.

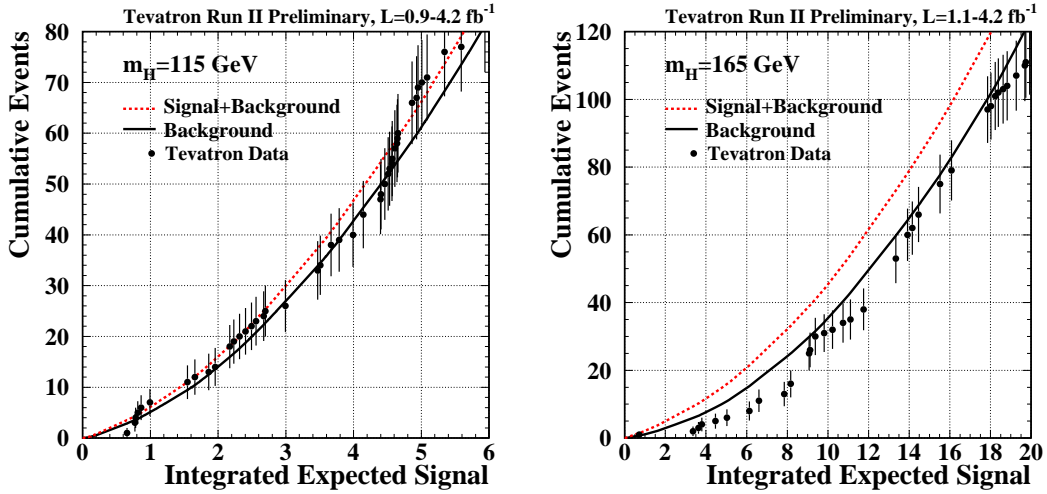


FIG. 2: Integrated distributions of s/b , starting at the high s/b side. The total signal+background and background-only integrals are shown separately, along with the data sums. Data are only shown for bins that have data events in them.

$$\mathcal{L}(R, \vec{s}, \vec{b} | \vec{n}, \vec{\theta}) \times \pi(\vec{\theta}) = \prod_{i=1}^{N_C} \prod_{j=1}^{N_{bins}} \mu_{ij}^{n_{ij}} e^{-\mu_{ij}} / n_{ij}! \times \prod_{k=1}^{n_{np}} e^{-\theta_k^2/2} \quad (1)$$

where the first product is over the number of channels (N_C), and the second product is over histogram bins containing n_{ij} events, binned in ranges of the final discriminants used for individual analyses, such as the dijet mass, neural-

network outputs, or matrix-element likelihoods. The parameters that contribute to the expected bin contents are $\mu_{ij} = R \times s_{ij}(\vec{\theta}) + b_{ij}(\vec{\theta})$ for the channel i and the histogram bin j , where s_{ij} and b_{ij} represent the expected background and signal in the bin, and R is a scaling factor applied to the signal to test the sensitivity level of the experiment. Truncated Gaussian priors are used for each of the nuisance parameters θ_k , which define the sensitivity of the predicted signal and background estimates to systematic uncertainties. These can take the form of uncertainties on overall rates, as well as the shapes of the distributions used for combination. These systematic uncertainties can be far larger than the expected SM signal, and are therefore important in the calculation of limits. The truncation is applied so that no prediction of any signal or background in any bin is negative. The posterior density function is then integrated over all parameters (including correlations) except for R , and a 95% credibility level upper limit on R is estimated by calculating the value of R that corresponds to 95% of the area of the resulting distribution.

B. Modified Frequentist Method

The Modified Frequentist technique relies on the CL_s method, using a log-likelihood ratio (LLR) as test statistic [2]:

$$LLR = -2 \ln \frac{p(\text{data}|H_1)}{p(\text{data}|H_0)}, \quad (2)$$

where H_1 denotes the test hypothesis, which admits the presence of SM backgrounds and a Higgs boson signal, while H_0 is the null hypothesis, for only SM backgrounds. The probabilities p are computed using the best-fit values of the nuisance parameters for each event, separately for each of the two hypotheses, and include the Poisson probabilities of observing the data multiplied by Gaussian constraints for the values of the nuisance parameters. This technique extends the LEP procedure [40] which does not involve a fit, in order to yield better sensitivity when expected signals are small and systematic uncertainties on backgrounds are large [41].

The CL_s technique involves computing two p -values, CL_{s+b} and CL_b . The latter is defined by

$$1 - CL_b = p(LLR \leq LLR_{\text{obs}}|H_0), \quad (3)$$

where LLR_{obs} is the value of the test statistic computed for the data. $1 - CL_b$ is the probability of observing a signal-plus-background-like outcome without the presence of signal, i.e. the probability that an upward fluctuation of the background provides a signal-plus-background-like response as observed in data. The other p -value is defined by

$$CL_{s+b} = p(LLR \geq LLR_{\text{obs}}|H_1), \quad (4)$$

and this corresponds to the probability of a downward fluctuation of the sum of signal and background in the data. A small value of CL_{s+b} reflects inconsistency with H_1 . It is also possible to have a downward fluctuation in data even in the absence of any signal, and a small value of CL_{s+b} is possible even if the expected signal is so small that it cannot be tested with the experiment. To minimize the possibility of excluding a signal to which there is insufficient sensitivity (an outcome expected 5% of the time at the 95% C.L., for full coverage), we use the quantity $CL_s = CL_{s+b}/CL_b$. If $CL_s < 0.05$ for a particular choice of H_1 , that hypothesis is deemed excluded at the 95% C.L.

Systematic uncertainties are included by fluctuating the predictions for signal and background rates in each bin of each histogram in a correlated way when generating the pseudoexperiments used to compute CL_{s+b} and CL_b .

C. Systematic Uncertainties

Systematic uncertainties differ between experiments and analyses, and they affect the rates and shapes of the predicted signal and background in correlated ways. The combined results incorporate the sensitivity of predictions to values of nuisance parameters, and include correlations, between rates and shapes, between signals and backgrounds, and between channels within experiments and between experiments. More on these issues can be found in the individual analysis notes [7] through [20]. Here we consider only the largest contributions and correlations between and within the two experiments.

1. Correlated Systematics between CDF and DØ

The uncertainty on the measurement of the integrated luminosity is 6% (CDF) and 6.1% (DØ). Of this value, 4% arises from the uncertainty on the inelastic $p\bar{p}$ scattering cross section, which is correlated between CDF and DØ. The uncertainty on the production rates for the signal, for top-quark processes ($t\bar{t}$ and single top) and for electroweak processes (WW , WZ , and ZZ) are taken as correlated between the two experiments. As the methods of measuring the multijet (“QCD”) backgrounds differ between CDF and DØ, there is no correlation assumed between these rates. Similarly, the large uncertainties on the background rates for W +heavy flavor (HF) and Z +heavy flavor are considered at this time to be uncorrelated, as both CDF and DØ estimate these rates using data control samples, but employ different techniques. The calibrations of fake leptons, unvetoes $\gamma \rightarrow e^+e^-$ conversions, b -tag efficiencies and mistag rates are performed by each collaboration using independent data samples and methods, hence are considered uncorrelated.

2. Correlated Systematic Uncertainties for CDF

The dominant systematic uncertainties for the CDF analyses are shown in Table IV for the $W^\pm H \rightarrow W^\pm b\bar{b}$ channels, in Table VI for the $(W, Z)H \rightarrow \cancel{E}_T b\bar{b}$ channels, in Table VIII for the $ZH \rightarrow \ell^+\ell^- b\bar{b}$ channels, in Table X for the $H \rightarrow W^+W^- \rightarrow \ell'^{\pm}\nu\ell'^{\mp}\nu$ channels, in Table XV for the $H \rightarrow \tau^+\tau^-$ channel, in Table IV C 3 for the $WH+ZH \rightarrow jjb\bar{b}$ channel, and in Table XI for the $WH \rightarrow WWW \rightarrow \ell'^{\pm}\ell'^{\pm}$ channel. Each source induces a correlated uncertainty across all CDF channels’ signal and background contributions which are sensitive to that source. For $H \rightarrow b\bar{b}$, the largest uncertainties on signal arise from a scale factor for b -tagging (5.3-16%), jet energy scale (1-20%) and MC modeling (2-10%). The shape dependence of the jet energy scale, b -tagging and uncertainties on gluon radiation (“ISR” and “FSR”) are taken into account for some analyses (see tables). For $H \rightarrow W^+W^-$, the largest uncertainty comes from MC modeling (5%). For simulated backgrounds, the uncertainties on the expected rates range from 11-40% (depending on background). The backgrounds with the largest systematic uncertainties are in general quite small. Such uncertainties are constrained by fits to the nuisance parameters, and they do not affect the result significantly. Because the largest background contributions are measured using data, these uncertainties are treated as uncorrelated for the $H \rightarrow b\bar{b}$ channels. For the $H \rightarrow W^+W^-$ channel, the uncertainty on luminosity is taken to be correlated between signal and background. The differences in the resulting limits when treating the remaining uncertainties as correlated or uncorrelated, is less than 5%.

3. Correlated Systematic Uncertainties for DØ

The dominant systematic uncertainties for DØ analyses are shown in Tables V, VII, IX, XII, XIII, XVII, and XIV. Each source induces a correlated uncertainty across all DØ channels sensitive to that source. The $H \rightarrow b\bar{b}$ analyses have an uncertainty on the b -tagging rate of 3-10% per tagged jet, and also an uncertainty on the jet energy and acceptance of 6-9% (jet identification or jet ID, energy scale, and jet resolution). The shape dependence of the uncertainty on W +jet modeling is taken into account in the limit setting, and has a small effect ($\sim 5\%$) on the final result. For the $H \rightarrow W^+W^-$ and $WH \rightarrow WW^+W^-$, the largest uncertainties are associated with lepton measurement and acceptance. These values range from 2-11% depending on the final state. The largest contributing factor to all analyses is the uncertainty on cross sections for simulated background, and is 6-18%. All systematic uncertainties arising from the same source are taken to be correlated between the different backgrounds and between signal and background.

TABLE IV: Systematic uncertainties on the signal contributions for CDF's $WH \rightarrow \ell\nu b\bar{b}$ tight (TDT) and loose (LDT) double tag, and single tag (ST) channels. Systematic uncertainties are listed by name, see the original references for a detailed explanation of their meaning and on how they are derived. Systematic uncertainties for WH shown in this table are obtained for $m_H = 115 \text{ GeV}/c^2$. Uncertainties are relative, in percent and are symmetric unless otherwise indicated.

CDF: tight double-tag (TDT) $WH \rightarrow \ell\nu b\bar{b}$

Contribution	W+HF	Mistags	Top	Diboson	Non-W	WH
Luminosity ($\sigma_{\text{inel}}(p\bar{p})$)	0	0	3.8	3.8	0	3.8
Luminosity Monitor	0	0	4.4	4.4	0	4.4
Lepton ID	0	0	2	2	0	2
Jet Energy Scale	0	0	0	0	0	2
Mistag Rate	0	9.0	0	0	0	0
B-Tag Efficiency	0	0	8.4	8.4	0	8.4
$t\bar{t}$ Cross Section	0	0	10	0	0	0
Diboson Rate	0	0	0	11.5	0	0
Signal Cross Section	0	0	0	0	0	5
HF Fraction in W+jets	30.1	0	0	0	0	0
ISR+FSR+PDF	0	0	0	0	0	5.6
QCD Rate	0	0	0	0	40	0

CDF: loose double-tag (LDT) $WH \rightarrow \ell\nu b\bar{b}$

Contribution	W+HF	Mistags	Top	Diboson	Non-W	WH
Luminosity ($\sigma_{\text{inel}}(p\bar{p})$)	0	0	3.8	3.8	0	3.8
Luminosity Monitor	0	0	4.4	4.4	0	4.4
Lepton ID	0	0	2	2	0	2
Jet Energy Scale	0	0	0	0	0	2
Mistag Rate	0	8.0	0	0	0	0
B-Tag Efficiency	0	0	9.1	9.1	0	9.1
$t\bar{t}$ Cross Section	0	0	10	0	0	0
Diboson Rate	0	0	0	11.5	0	0
Signal Cross Section	0	0	0	0	0	5
HF Fraction in W+jets	30.1	0	0	0	0	0
ISR+FSR+PDF	0	0	0	0	0	4.3
QCD Rate	0	0	0	0	40	0

CDF: single tag (ST) $WH \rightarrow \ell\nu b\bar{b}$

Contribution	W+HF	Mistags	Top	Diboson	Non-W	WH
Luminosity ($\sigma_{\text{inel}}(p\bar{p})$)	0	0	3.8	3.8	0	3.8
Luminosity Monitor	0	0	4.4	4.4	0	4.4
Lepton ID	0	0	2	2	0	2
Jet Energy Scale	0	0	0	0	0	2
Mistag Rate	0	13.3	0	0	0	0
B-Tag Efficiency	0	0	3.5	3.5	0	3.5
$t\bar{t}$ Cross Section	0	0	10	0	0	0
Diboson Rate	0	0	0	11.5	0	0
Signal Cross Section	0	0	0	0	0	5
HF Fraction in W+jets	30.1	0	0	0	0	0
ISR+FSR+PDF	0	0	0	0	0	3.1
QCD Rate	0	0	0	0	40	0

TABLE V: Systematic uncertainties on the signal contributions for $D\bar{O}$'s $WH \rightarrow \ell\nu b\bar{b}$ single (ST) and double tag (DT) channels, $WH \rightarrow \tau\nu b\bar{b}$, and $VH \rightarrow \tau\tau b\bar{b}/q\bar{q}\tau\tau$. Systematic uncertainties are listed by name, see the original references for a detailed explanation of their meaning and on how they are derived. Systematic uncertainties for WH shown in this table are obtained for $m_H = 115 \text{ GeV}/c^2$. Uncertainties are relative, in percent and are symmetric unless otherwise indicated.

$D\bar{O}$: Single Tag (ST) $WH \rightarrow \ell\nu b\bar{b}$ Analysis

Contribution	WZ/WW	Wbb/Wcc	Wjj/Wcj	$t\bar{t}$	single top	Multijet	WH
Luminosity	6	6	6	6	6	0	6
Trigger eff.	3-5	3-5	3-5	3-5	3-5	0	3-5
EM ID/Reco eff./resol.	5	5	5	5	5	0	5
Muon ID/Reco eff./resol.	5	5	5	5	5	0	5
Jet ID/Reco eff.	3	3	3	3	3	0	3
Jet Energy Scale	3	4	3	4	2	0	3
Jet mult./frag./modeling	0	11	9	5	5	0	5
b -tagging/taggability	4	4	15	4	4	0	4
Cross Section	6	9	9	10	10	0	6
Heavy-Flavor K-factor	0	20	0	0	0	0	0
Instrumental-WH	0	0	-6	0	0	26	0

$D\bar{O}$: Double Tag (DT) $WH \rightarrow \ell\nu b\bar{b}$ Analysis

Contribution	WZ/WW	Wbb/Wcc	Wjj/Wcj	$t\bar{t}$	single top	Multijet	WH
Luminosity	6	6	6	6	6	0	6
Trigger eff.	3-5	3-5	3-5	3-5	3-5	0	3-5
EM ID/Reco eff./resol.	5	5	5	5	5	0	5
Muon ID/Reco eff./resol.	5	5	5	5	5	0	5
Jet ID/Reco eff.	3	3	3	3	3	0	3
Jet Energy Scale	3	4	3	4	2	0	3
Jet mult./frag./modeling	0	11	9	5	5	0	5
b -tagging/taggability	8	8	25	8	8	0	8
Cross Section	6	9	9	10	10	0	6
Heavy-Flavor K-factor	0	20	0	0	0	0	0
Instrumental-WH	0	0	-6	0	0	26	0

$D\bar{O}$: $WH \rightarrow \tau\nu b\bar{b}$ and $VH \rightarrow \tau\tau b\bar{b}/q\bar{q}\tau\tau$ analyses

Contribution	background	WH $\tau\nu b\bar{b}$	background	VH $\tau\tau b\bar{b}/q\bar{q}\tau\tau$
Luminosity	6	6	6	6
Trigger eff.	6	6	3	3
μ ID	-	-	5	5
τ ID	5-6	5-6	3	3
τ energy scale	3	3	4	4
Jet ID/Reco eff.	2-5	2-5	2-5	2-5
Jet Resolution	4	1	4	1
Jet Energy Scale	1	1	8	8
b -tagging/taggability	4	1	4	1
Cross Section	6-18	6	6-18	6
Heavy-Flavor K-factor	30	0	30	0
Instrumental-WH	35-100	0	35-100	0

TABLE VI: Systematic uncertainties for CDF's $ZH \rightarrow \nu\bar{\nu}b\bar{b}$ tight (TDT and loose (LDT) double-tag, and single-tag (ST) channel. Systematic uncertainties are listed by name, see the original references for a detailed explanation of their meaning and on how they are derived. Systematic uncertainties for ZH and WH shown in this table are obtained for $m_H = 120 \text{ GeV}/c^2$. Uncertainties are relative, in percent and are symmetric unless otherwise indicated.

CDF: $ZH \rightarrow \nu\bar{\nu}b\bar{b}$ tight double-tag (TDT) channel

	ZH	WH	Multijet	Top Pair	S. Top	Di-boson	W + h.f.	Z + h.f.
<i>Correlated uncertainties</i>								
Luminosity	3.8	3.8		3.8	3.8	3.8	3.8	3.8
Lumi Monitor	4.4	4.4		4.4	4.4	4.4	4.4	4.4
Tagging SF	8.6	8.6		8.6	8.6	8.6	8.6	8.6
Trigger Eff. (shape)	1.0	1.2	1.1	0.7	1.1	1.6	1.7	1.3
Lepton Veto	2.0	2.0		2.0	2.0	2.0	2.0	2.0
PDF Acceptance	2.0	2.0		2.0	2.0	2.0	2.0	2.0
JES (shape)	+3.0 -3.0	+3.5 -4.7	-4.0 +3.8	+1.1 -1.1	+2.4 -4.7	+8.2 -6.1	+7.3 -11.8	+6.5 -8.3
ISR		+4.4						
FSR		+3.7 +1.8 +4.4						
<i>Uncorrelated uncertainties</i>								
Cross-Section	5	5		10	10	11.5	40	40
Multijet Norm. (shape)			20.6					

CDF: $ZH \rightarrow \nu\bar{\nu}b\bar{b}$ loose double-tag (LDT) channel

	ZH	WH	Multijet	Top Pair	S. Top	Di-boson	W + h.f.	Z + h.f.
<i>Correlated uncertainties</i>								
Luminosity	3.8	3.8		3.8	3.8	3.8	3.8	3.8
Lumi Monitor	4.4	4.4		4.4	4.4	4.4	4.4	4.4
Tagging SF	12.4	12.4		12.4	12.4	12.4	12.4	12.4
Trigger Eff. (shape)	1.2	1.3	1.1	0.7	1.2	1.2	1.8	1.3
Lepton Veto	2.0	2.0		2.0	2.0	2.0	2.0	2.0
PDF Acceptance	2.0	2.0		2.0	2.0	2.0	2.0	2.0
JES (shape)	+3.7 -3.7	+4.0 -4.0	-5.4 +5.2	+1.1 -0.7	+4.2 -4.2	+7.0 -7.0	+1.3 -7.6	+6.2 -7.1
ISR		+1.4 -2.9						
FSR		+5.3 +2.5						
<i>Uncorrelated uncertainties</i>								
Cross-Section	5.0	5.0		10	10	11.5	40	40
Multijet Norm. (shape)			15.6					

CDF: $ZH \rightarrow \nu\bar{\nu}b\bar{b}$ single-tag (ST) channel

	ZH	WH	Multijet	Top Pair	S. Top	Di-boson	W + h.f.	Z + h.f.
<i>Correlated uncertainties</i>								
Luminosity	3.8	3.8		3.8	3.8	3.8	3.8	3.8
Lumi Monitor	4.4	4.4		4.4	4.4	4.4	4.4	4.4
Tagging SF	4.3	4.3		4.3	4.3	4.3	4.3	4.3
Trigger Eff. (shape)	0.9	1.1	1.1	0.7	1.1	1.3	2.0	1.4
Lepton Veto	2.0	2.0		2.0	2.0	2.0	2.0	2.0
PDF Acceptance	2.0	2.0		2.0	2.0	2.0	2.0	2.0
JES (shape)	+3.8 -3.8	+3.8 -3.8	-5.2 +5.6	+0.7 -0.8	+4.6 -4.6	+7.0 -5.6	+12.4 -12.7	+8.3 -8.1
ISR		-1.0 -1.5						
FSR		+2.0 -0.1						
<i>Uncorrelated uncertainties</i>								
Cross-Section	5.0	5.0		10	10	11.5	40	40
Multijet Norm. (shape)			5.5					

TABLE VII: Systematic uncertainties on the contributions for $D\mathcal{O}$'s $ZH \rightarrow \nu\nu b\bar{b}$ double-tag (DT) channel. Systematic uncertainties are listed by name, see the original references for a detailed explanation of their meaning and on how they are derived. Systematic uncertainties for ZH , WH shown in this table are obtained for $m_H = 115 \text{ GeV}/c^2$. Uncertainties are relative, in percent and are symmetric unless otherwise indicated.

D \mathcal{O} : Double Tag (DT) $ZH \rightarrow \nu\nu b\bar{b}$ Analysis

Contribution	WZ/ZZ	Z+jets	W+jets	$t\bar{t}$	ZH,WH
Luminosity	6	6	6	6	6
Trigger eff.	5	5	5	5	5
Jet Energy Scale	3	3	3	3	2
Jet ID/resolution.	2	2	2	2	2
b -tagging/taggability	6	6	6	6	6
Cross Section	6	15	15	18	6
Heavy Flavour K-factor	-	50	50	-	-

TABLE IX: Systematic uncertainties on the contributions for DØ's $ZH \rightarrow \ell^+ \ell^- b\bar{b}$ single-tag (ST) channel. Systematic uncertainties are listed by name, see the original references for a detailed explanation of their meaning and on how they are derived. Systematic uncertainties for ZH shown in this table are obtained for $m_H = 115 \text{ GeV}/c^2$. Uncertainties are relative, in percent and are symmetric unless otherwise indicated.

DØ: Single Tag (ST) $ZH \rightarrow \ell b\bar{b}$ Analysis

Contribution	WZ/ZZ	Zbb/Zcc	Zjj	$t\bar{t}$	Multijet	ZH
Luminosity	6	6	6	6	0	6
EM ID/Reco eff.	2	2	2	2	0	2
Muon ID/Reco eff.	2	2	2	2	0	2
Jet ID/Reco eff.	2	2	2	2	0	2
Jet Energy Scale (shape dep.)	5	5	5	5	0	5
b -tagging/taggability	5	5	5	5	0	5
Cross Section	6	30	6	10	0	6
MC modeling	0	4	4	0	0	0
Instrumental-ZH	0	0	0	0	50	0

DØ: Double Tag (DT) $ZH \rightarrow \ell b\bar{b}$ Analysis

Contribution	WZ/ZZ	Zbb/Zcc	Zjj	$t\bar{t}$	Multijet	ZH
Luminosity	6	6	6	6	0	6
EM ID/Reco eff.	2	2	2	2	0	2
Muon ID/Reco eff.	2	2	2	2	0	2
Jet ID/Reco eff.	2	2	2	2	0	2
Jet Energy Scale (shape dep.)	5	5	5	5	0	5
b -tagging/taggability	10	10	10	10	0	10
Cross Section	6	30	6	10	0	6
MC modeling	0	4	4	0	0	0
Instrumental-ZH	0	0	0	0	50	0

TABLE X: Systematic uncertainties on the contributions for CDF's $H \rightarrow W^+W^- \rightarrow \ell^\pm \ell'^\mp$ channels with zero, one, and two or more associated jets. These channels are sensitive to WH, ZH or VBF signals. Systematic uncertainties are listed by name, see the original references for a detailed explanation of their meaning and on how they are derived. Systematic uncertainties for H shown in this table are obtained for $m_H = 165 \text{ GeV}/c^2$. Uncertainties are relative, in percent and are symmetric unless otherwise indicated. Uncertainties in bold are correlated across jet bins but not across channels. Uncertainties in italics are correlated across jet bins and across appropriate channels. Monte Carlo statistical uncertainties in each bin of each template are considered as independent systematic uncertainties.

CDF: $H \rightarrow W^+W^- \rightarrow \ell^\pm \ell'^\mp$ channels with no associated jet											
Uncertainty Source	WW	WZ	ZZ	$t\bar{t}$	DY	$W\gamma$	$W+\text{jet(s)}$	$gg \rightarrow H$			
Cross Section	<i>6.0</i>	<i>6.0</i>	<i>6.0</i>	<i>10.0</i>	5.0	<i>10.0</i>		<i>12.0</i>			
Scale (leptons)								2.5			
Scale (jets)								4.6			
PDF Model (leptons)	1.9	2.7	2.7	2.1	4.1	2.2		1.5			
PDF Model (jets)								0.9			
Higher-order Diagrams	5.5	10.0	10.0	10.0	5.0	10.0					
Missing Et Modeling	1.0	1.0	1.0	1.0	21.0	1.0		1.0			
Conversion Modeling						20.0					
Jet Fake Rates (Low/High S/B)								21.5/27.7			
$W\gamma$ +jet modeling						<i>4.0</i>					
Lepton ID Efficiencies	2.0	1.7	2.0	2.0	1.9	1.4		1.9			
Trigger Efficiencies	2.1	2.1	2.1	2.0	3.4	7.0		3.3			
Luminosity	3.8	3.8	3.8	3.8	3.8	3.8		3.8			
Luminosity Monitor	4.4	4.4	4.4	4.4	4.4	4.4		4.4			

CDF: $H \rightarrow W^+W^- \rightarrow \ell^\pm \ell'^\mp$ channels with one associated jet											
Uncertainty Source	WW	WZ	ZZ	$t\bar{t}$	DY	$W\gamma$	$W+\text{jet(s)}$	$gg \rightarrow H$	WH	ZH	VBF
Cross Section	<i>6.0</i>	<i>6.0</i>	<i>6.0</i>	<i>10.0</i>	5.0	<i>10.0</i>		<i>12.0</i>	<i>5.0</i>	<i>5.0</i>	<i>10.0</i>
Scale (leptons)								2.8			
Scale (jets)								-5.1			
PDF Model (leptons)	1.9	2.7	2.7	2.1	4.1	2.2		1.7	1.2	0.9	2.2
PDF Model (jets)								-1.9			
Higher-order Diagrams	5.5	10.0	10.0	10.0	5.0	10.0			<i>10.0</i>	<i>10.0</i>	<i>10.0</i>
Missing Et Modeling	1.0	1.0	1.0	1.0	30.0	1.0		1.0	1.0	1.0	1.0
Conversion Modeling						20.0					
Jet Fake Rates (Low/High S/B)								22.2/31.5			
$W\gamma$ +jet modeling						<i>15.0</i>					
MC Run Dependence	1.8			2.2		2.2		2.6	2.6	1.9	2.8
Lepton ID Efficiencies	2.0	2.0	2.2	1.8	2.0	2.0		1.9	1.9	1.9	1.9
Trigger Efficiencies	2.1	2.1	2.1	2.0	3.4	7.0		3.3	2.1	2.1	3.3
Luminosity	3.8	3.8	3.8	3.8	3.8	3.8		3.8	3.8	3.8	3.8
Luminosity Monitor	4.4	4.4	4.4	4.4	4.4	4.4		4.4	4.4	4.4	4.4

CDF: $H \rightarrow W^+W^- \rightarrow \ell^\pm \ell'^\mp$ channels with two or more associated jets											
Uncertainty Source	WW	WZ	ZZ	$t\bar{t}$	DY	$W\gamma$	$W+\text{jet(s)}$	$gg \rightarrow H$	WH	ZH	VBF
Cross Section	<i>6.0</i>	<i>6.0</i>	<i>6.0</i>	<i>10.0</i>	5.0	<i>10.0</i>		<i>12.0</i>	<i>5.0</i>	<i>5.0</i>	<i>10.0</i>
Scale (leptons)								3.1			
Scale (jets)								-8.7			
PDF Model (leptons)	1.9	2.7	2.7	2.1	4.1	2.2		2.0	1.2	0.9	2.2
PDF Model (jets)								-2.8			
Higher-order Diagrams	10.0	10.0	10.0	10.0	10.0	10.0			<i>10.0</i>	<i>10.0</i>	<i>10.0</i>
Missing Et Modeling	1.0	1.0	1.0	1.0	32.0	1.0		1.0	1.0	1.0	1.0
Conversion Modeling						20.0					
b -tag Veto				7.0							
Jet Fake Rates								27.1			
$W\gamma$ +jet modeling						<i>20.0</i>					
MC Run Dependence	1.0			1.0		1.0		1.7	2.0	1.9	2.6
Lepton ID Efficiencies	1.9	2.9	1.9	1.9	1.9	1.9		1.9	1.9	1.9	1.9
Trigger Efficiencies	2.1	2.1	2.1	2.0	3.4	7.0		3.3	2.1	2.1	3.3
Luminosity	3.8	3.8	3.8	3.8	3.8	3.8		3.8	3.8	3.8	3.8
Luminosity Monitor	4.4	4.4	4.4	4.4	4.4	4.4		4.4	4.4	4.4	4.4

TABLE XI: Systematic uncertainties on the contributions for CDF's $WH \rightarrow WWW \rightarrow \ell^\pm \ell'^\pm$ channel. Systematic uncertainties are listed by name, see the original references for a detailed explanation of their meaning and on how they are derived. Systematic uncertainties for ZH , WH shown in this table are obtained for $m_H = 165 \text{ GeV}/c^2$. Uncertainties are relative, in percent and are symmetric unless otherwise indicated. Uncertainties in bold are correlated across jet bins but not across channels. Uncertainties in italics are correlated across jet bins and across appropriate channels. Monte Carlo statistical uncertainties in each bin of each template are considered as independent systematic uncertainties.

CDF: $WH \rightarrow WWW \rightarrow \ell^\pm \ell'^\pm$ Analysis.

Uncertainty Source	WW	WZ	ZZ	$t\bar{t}$	DY	$W\gamma$	$W+\text{jet(s)}$	WH	ZH
Cross Section	<i>6.0</i>	<i>6.0</i>	<i>6.0</i>	<i>10.0</i>	5.0	<i>10.0</i>		<i>5.0</i>	<i>5.0</i>
PDF Model (leptons)	1.9	2.7	2.7	2.1	4.1	2.2		1.2	0.9
PDF Model (jets)									
Higher-order Diagrams	10.0	10.0	10.0	10.0	10.0	10.0		<i>10.0</i>	<i>10.0</i>
Missing Et Modeling	1.0	1.0	1.0	1.0	20.0	1.0		1.0	1.0
Conversion Modeling						20.0			
$W\gamma$ +jet modeling						<i>16.0</i>			
Jet Fake Rates							30.0		
Charge Misassignment	16.5			16.5	16.5				
MC Run Dependence	1.9			1.0		2.4			
Lepton ID Efficiencies	1.9	2.9	1.9	1.9	1.9	1.9		1.9	1.9
Trigger Efficiencies	2.1	2.1	2.1	2.0	3.4	7.0		2.1	2.1
Luminosity	3.8	3.8	3.8	3.8	3.8	3.8		3.8	3.8
Luminosity Monitor	4.4	4.4	4.4	4.4	4.4	4.4		4.4	4.4

TABLE XII: Systematic uncertainties on the contributions for DØ's $WH \rightarrow WWW \rightarrow \ell^\pm \ell'^\pm$ channel. Systematic uncertainties are listed by name, see the original references for a detailed explanation of their meaning and on how they are derived. Systematic uncertainties for WH shown in this table are obtained for $m_H = 165 \text{ GeV}/c^2$. Uncertainties are relative, in percent and are symmetric unless otherwise indicated.

DØ: $WH \rightarrow WWW \rightarrow \ell^\pm \ell'^\pm$ Run IIa Analysis.

Contribution	WZ/ZZ	Charge flips	Multijet	WH
Luminosity	6	0	0	6
Trigger eff.	5	0	0	5
Lepton ID/Reco. eff	10	0	0	10
Cross Section	7	0	0	6
Normalization	6	0	0	0
Instrumental- ee (ee final state)	0	32	15	0
Instrumental- $e\mu$ ($e\mu$ final state)	0	0	18	0
Instrumental- $\mu\mu$ ($\mu\mu$ final state)	0	$^{+290}_{-100}$	32	0

TABLE XIII: Systematic uncertainties on the contributions for DØ's $H \rightarrow WW \rightarrow \ell^\pm \ell'^\mp$ channels. Systematic uncertainties are listed by name, see the original references for a detailed explanation of their meaning and on how they are derived. Systematic uncertainties shown in this table are obtained for the $m_H = 165 \text{ GeV}/c^2$ Higgs selection. Uncertainties are relative, in percent and are symmetric unless otherwise indicated.

DØ: $H \rightarrow WW \rightarrow e^\pm e^\mp$ Analysis

Contribution	Diboson	$Z/\gamma^* \rightarrow \ell\ell$	$W + jet/\gamma$	$t\bar{t}$	Multijet	H
Lepton ID	3	3	3	3	–	3
Momentum resolution	1	1	1	1	–	1
Jet Energy Scale	5	2	0	5	–	3
Jet identification	5	1	0	5	–	3
Cross Section/normalization	6	6	13	10	2	6
Modeling	3	5	0	0	0	3

DØ: $H \rightarrow WW \rightarrow e^\pm \mu^\mp$ Analysis

Contribution	Diboson	$Z/\gamma^* \rightarrow \ell\ell$	$W + jet/\gamma$	$t\bar{t}$	Multijet	H
Lepton ID	1	1	1	1	–	1
Momentum resolution	1	4	1	0	–	1
Jet Energy Scale	2	2	3	5	–	3
Jet identification	0	4	1	4	–	1
Cross Section/normalization	6	6	13	10	13	6
Modeling	1	3	0	0	0	2

DØ: $H \rightarrow WW \rightarrow \mu^\pm \mu^\mp$ Analysis

Contribution	Diboson	$Z/\gamma^* \rightarrow \ell\ell$	$W + jet/\gamma$	$t\bar{t}$	Multijet	H
trigger	2	2	2	2	–	2
Lepton ID	3	3	3	3	–	3
Momentum resolution	2	2	2	2	–	2
Jet Energy Scale	5	2	0	5	–	3
Cross Section/normalization	6	6	13	10	2	6
Modeling	3	5	0	0	0	3

TABLE XIV: Systematic uncertainties on the contributions for DØ’s $t\bar{t}H \rightarrow t\bar{t}b\bar{b}$ channel. Systematic uncertainties for ZH , WH shown in this table are obtained for $m_H = 115 \text{ GeV}/c^2$. Systematic uncertainties are listed by name, see the original references for a detailed explanation of their meaning and on how they are derived. Uncertainties are relative, in percent and are symmetric unless otherwise indicated.

DØ: $t\bar{t}H \rightarrow t\bar{t}b\bar{b}$ Analysis

Contribution	background	$t\bar{t}H$
Luminosity	6	6
lepton ID efficiency	2–3	2–3
Event preselection	1	1
W +jet modeling	15	-
Cross Section	10–50	10

TABLE XV: Systematic uncertainties on the contributions for CDF’s $H \rightarrow \tau^+\tau^-$ channels. Systematic uncertainties are listed by name, see the original references for a detailed explanation of their meaning and on how they are derived. Systematic uncertainties for H shown in this table are obtained for $m_H = 115 \text{ GeV}/c^2$. Uncertainties are relative, in percent and are symmetric unless otherwise indicated. The systematic uncertainty called “Normalization” includes effects of the inelastic $p\bar{p}$ cross section, the luminosity monitor acceptance, and the lepton trigger acceptance. It is considered to be entirely correlated with the luminosity uncertainty.

CDF: $H \rightarrow \tau^+\tau^-$ Analysis

Contribution	$Z/\gamma^* \rightarrow \tau\tau$	$Z/\gamma^* \rightarrow \ell\ell$	$t\bar{t}$	diboson	jet $\rightarrow \tau$	W+jet	WH	ZH	VBF	$gg \rightarrow H$
Luminosity	3.8	3.8	3.8	3.8	-	-	3.8	3.8	3.8	3.8
Luminosity Monitor	4.4	4.4	4.4	4.4	-	-	4.4	4.4	4.4	4.4
e, μ Trigger	1	1	1	1	-	-	1	1	1	1
τ Trigger	3	3	3	3	-	-	3	3	3	3
e, μ, τ ID	3	3	3	3	-	-	3	3	3	3
PDF Uncertainty	1	1	1	1	-	-	1	1	1	1
ISR/FSR	-	-	-	-	-	-	2/0	1/1	3/1	12/1
JES (shape)	16	13	2	10	-	-	3	3	4	14
Cross Section or Norm.	2	2	10	11.5	-	15	5	5	10	10
MC model	20	10	-	-	-	-	-	-	-	-

TABLE XVI: Systematic uncertainties summary for CDF’s $WH + ZH \rightarrow jjb\bar{b}$ channel. Systematic uncertainties are listed by name, see the original references for a detailed explanation of their meaning and on how they are derived. Uncertainties with provided shape systematics are labeled with “s”. Systematic uncertainties for H shown in this table are obtained for $m_H = 115 \text{ GeV}/c^2$. Uncertainties are relative, in percent and are symmetric unless otherwise indicated. The cross section uncertainties are uncorrelated with each other (except for single top and $t\bar{t}$, which are treated as correlated). The QCD uncertainty is also uncorrelated with other channels’ QCD rate uncertainties.

CDF: $WH + ZH \rightarrow jjb\bar{b}$ Analysis

	QCD	$t\bar{t}$	$Wb\bar{b}$	WZ	Single Top	Z+jets	WH	ZH
Interpolation	0s	-	-	-	-	-	-	-
MC Modeling	0s	-	-	-	-	-	18s	16s
Cross Section	10	10	30	6	10	30	5	5

TABLE XVII: Systematic uncertainties on the contributions for DØ's $H \rightarrow \gamma\gamma$ channels. Systematic uncertainties for ZH , WH shown in this table are obtained for $m_H = 115 \text{ GeV}/c^2$. Systematic uncertainties are listed by name, see the original references for a detailed explanation of their meaning and on how they are derived. Uncertainties are relative, in percent and are symmetric unless otherwise indicated.

DØ: $H \rightarrow \gamma\gamma$ Analysis

Contribution	background	H
Luminosity	6	6
Acceptance	–	2
electron ID efficiency	2	2
electron track-match inefficiency	10–20	–
Photon ID efficiency	7	7
Photon energy scale	–	2
Acceptance	–	2
γ -jet and jet-jet fakes	26	–
Cross Section (Z)	4	6
Background subtraction	8–14	–

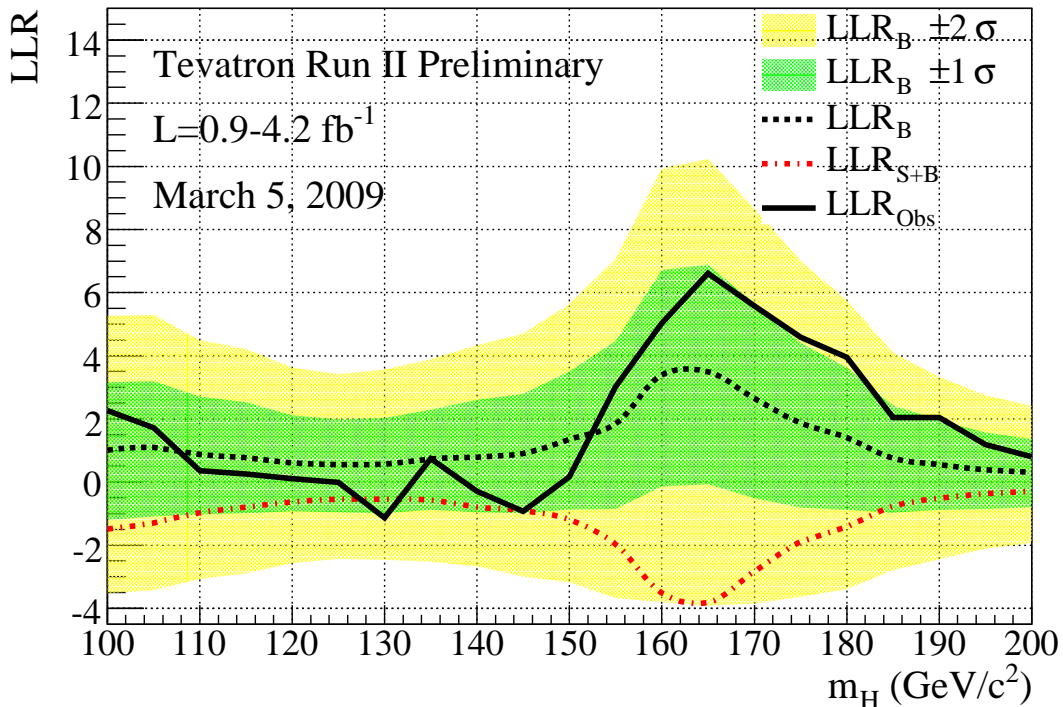


FIG. 3: Distributions of the log-likelihood ratio (LLR) as a function of Higgs mass obtained with the CL_s method for the combination of all CDF and $D\bar{O}$ analyses.

V. COMBINED RESULTS

Before extracting the combined limits we study the distributions of the log-likelihood ratio (LLR) for different hypotheses, to check the expected sensitivity across the mass range tested. Figure 3 displays the LLR distributions for the combined analyses as a function of m_H . Included are the results for the background-only hypothesis (LLR_b), the signal-plus-background hypothesis (LLR_{s+b}), and for the data (LLR_{obs}). The shaded bands represent the 1 and 2 standard deviation (σ) departures for LLR_b .

These distributions can be interpreted as follows: The separation between LLR_b and LLR_{s+b} provides a measure of the discriminating power of the search; the size of the 1- and 2- σ LLR_b bands provides an estimate of how sensitive the analysis is to a signal-plus-background-like fluctuation in data, taking account of the systematic uncertainties; the value of LLR_{obs} relative to LLR_{s+b} and LLR_b indicates whether the data distribution appears to be more signal-plus-background-like (i.e. closer to the LLR_{s+b} distribution, which is negative by construction) or background-like; the significance of any departures of LLR_{obs} from LLR_b can be evaluated by the width of the LLR_b bands.

Using the combination procedures outlined in Section III, we extract limits on SM Higgs boson production $\sigma \times B(H \rightarrow X)$ in $p\bar{p}$ collisions at $\sqrt{s} = 1.96$ TeV for $m_H = 100 - 200$ GeV/ c^2 . To facilitate comparisons with the standard model and to accommodate analyses with different degrees of sensitivity, we present our results in terms of the ratio of obtained limits to cross section in the SM, as a function of Higgs boson mass, for test masses for which both experiments have performed dedicated searches in different channels. A value of the combined limit ratio which

is less than or equal to one would indicate that that particular Higgs boson mass is excluded at the 95% C.L.

The combinations of results of each single experiment, as used in this Tevatron combination, yield the following ratios of 95% C.L. observed (expected) limits to the SM cross section: 3.6 (3.2) for CDF and 3.7 (3.9) for DØ at $m_H = 115 \text{ GeV}/c^2$, and 1.5 (1.6) for CDF and 1.3 (1.8) for DØ at $m_H = 165 \text{ GeV}/c^2$.

The ratios of the 95% C.L. expected and observed limit to the SM cross section are shown in Figure 4 for the combined CDF and DØ analyses. The observed and median expected ratios are listed for the tested Higgs boson masses in Table XVIII for $m_H \leq 150 \text{ GeV}/c^2$, and in Table XIX for $m_H \geq 150 \text{ GeV}/c^2$, as obtained by the Bayesian and the CL_S methods. In the following summary we quote only the limits obtained with the Bayesian method since they are slightly more conservative (based on the expected limits) for the quoted values, but all the equivalent numbers for the CL_S method can be retrieved from the tables. We obtain the observed (expected) values of 2.5 (2.4) at $m_H = 115 \text{ GeV}/c^2$, 0.99 (1.1) at $m_H = 160 \text{ GeV}/c^2$, 0.86 (1.1) at $m_H = 165 \text{ GeV}/c^2$, and 0.99 (1.4) at $m_H = 170 \text{ GeV}/c^2$. We exclude at the 95% C.L. the production of a standard model Higgs boson with mass between 160 and 170 GeV/c^2 . This result is obtained with both Bayesian and CL_S calculations.

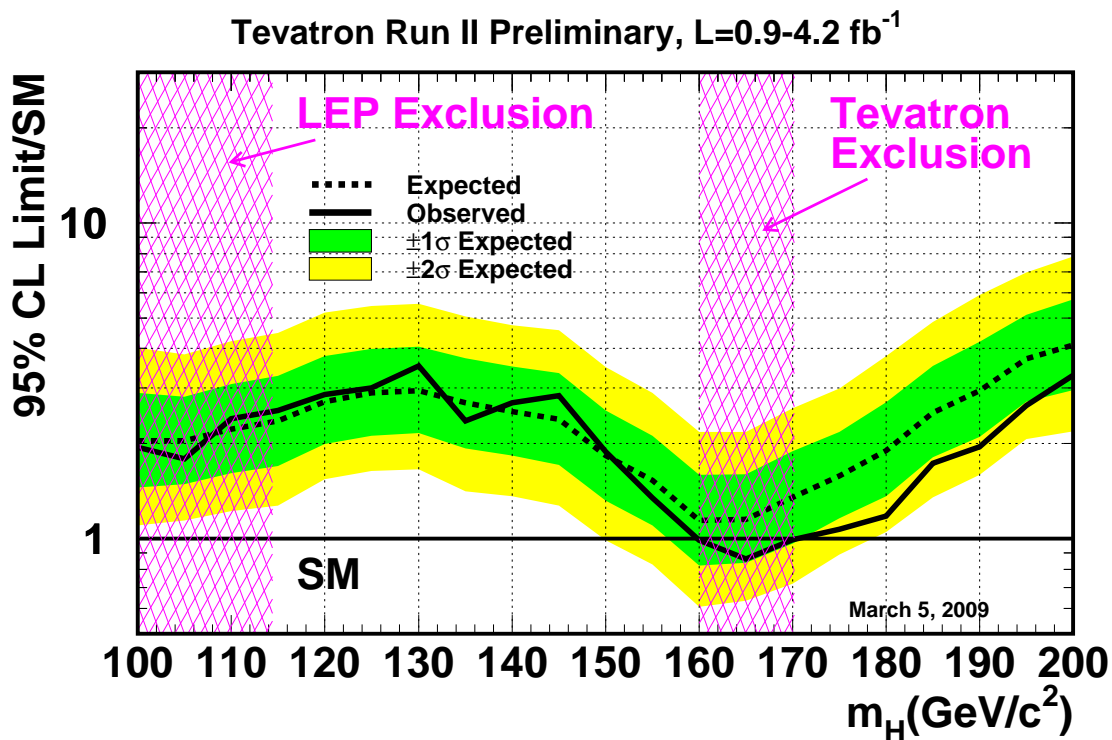


FIG. 4: Observed and expected (median, for the background-only hypothesis) 95% C.L. upper limits on the ratios to the SM cross section, as functions of the Higgs boson mass for the combined CDF and DØ analyses. The limits are expressed as a multiple of the SM prediction for test masses (every 5 GeV/c^2) for which both experiments have performed dedicated searches in different channels. The points are joined by straight lines for better readability. The bands indicate the 68% and 95% probability regions where the limits can fluctuate, in the absence of signal. The limits displayed in this figure are obtained with the Bayesian calculation.

TABLE XVIII: Ratios of median expected and observed 95% C.L. limit to the SM cross section for the combined CDF and $D\bar{O}$ analyses as a function of the Higgs boson mass in GeV/c^2 , obtained with the Bayesian and with the CL_S method.

Bayesian	100	105	110	115	120	125	130	135	140	145	150
Expected	2.0	2.0	2.2	2.4	2.7	2.9	2.9	2.7	2.5	2.4	1.8
Observed	1.9	1.8	2.4	2.5	2.8	3.0	3.5	2.4	2.7	2.8	1.9
CL_S	100	105	110	115	120	125	130	135	140	145	150
Expected	1.9	1.9	2.1	2.4	2.6	2.7	2.9	2.7	2.5	2.2	1.8
Observed	1.7	1.7	2.2	2.6	2.8	2.9	4.0	2.6	3.1	2.8	2.0

TABLE XIX: Ratios of median expected and observed 95% C.L. limit to the SM cross section for the combined CDF and $D\bar{O}$ analyses as a function of the Higgs boson mass in GeV/c^2 , obtained with the Bayesian and with the CL_S method.

Bayesian	155	160	165	170	175	180	185	190	195	200
Expected	1.5	1.1	1.1	1.4	1.6	1.9	2.2	2.7	3.5	4.2
Observed	1.4	0.99	0.86	0.99	1.1	1.2	1.7	2.0	2.6	3.3
CL_S	155	160	165	170	175	180	185	190	195	200
Expected	1.5	1.1	1.1	1.3	1.6	1.8	2.5	3.0	3.5	3.9
Observed	1.3	0.95	0.81	0.92	1.1	1.3	1.9	2.0	2.8	3.3

We also show in Figure 5 the $1-CL_S$ distribution as a function of the Higgs boson mass, at high mass ($\geq 150 \text{ GeV}/c^2$) which is directly interpreted as the level of exclusion at 95% C.L. of our search. Note that this figure is obtained using the CL_S method. The 90% C.L. line is also shown on the figure. We provide the Log-likelihood ratio (LLR) values for our combined Higgs boson search, as obtained using the CL_S method in table XX.

In summary, we have combined all available CDF and $D\bar{O}$ results on SM Higgs search, based on luminosities ranging from 0.9 to 4.2 fb^{-1} . Compared to our previous combination, new channels have been added and most previously used channels have been reanalyzed to gain sensitivity. We use the latest parton distribution functions and $gg \rightarrow H$ theoretical cross sections when comparing our limits to the SM predictions at high mass.

The 95% C.L. upper limits on Higgs boson production are a factor of 2.5 (0.86) times the SM cross section for a Higgs boson mass of $m_H = 115$ (165) GeV/c^2 . Based on simulation, the corresponding median expected upper limits are 2.4 (1.1). Standard Model branching ratios, calculated as functions of the Higgs boson mass, are assumed. These results extend significantly the individual limits of each collaboration and our previous combination. The mass range excluded at 95% C.L. for a SM Higgs has been extended to $160 < m_H < 170 \text{ GeV}/c^2$. The sensitivity of our combined search is expected to grow substantially in the near future with the additional luminosity already recorded at the Tevatron and not yet analyzed, and with additional improvements of our analysis techniques which will be propagated in the current and future analyses.

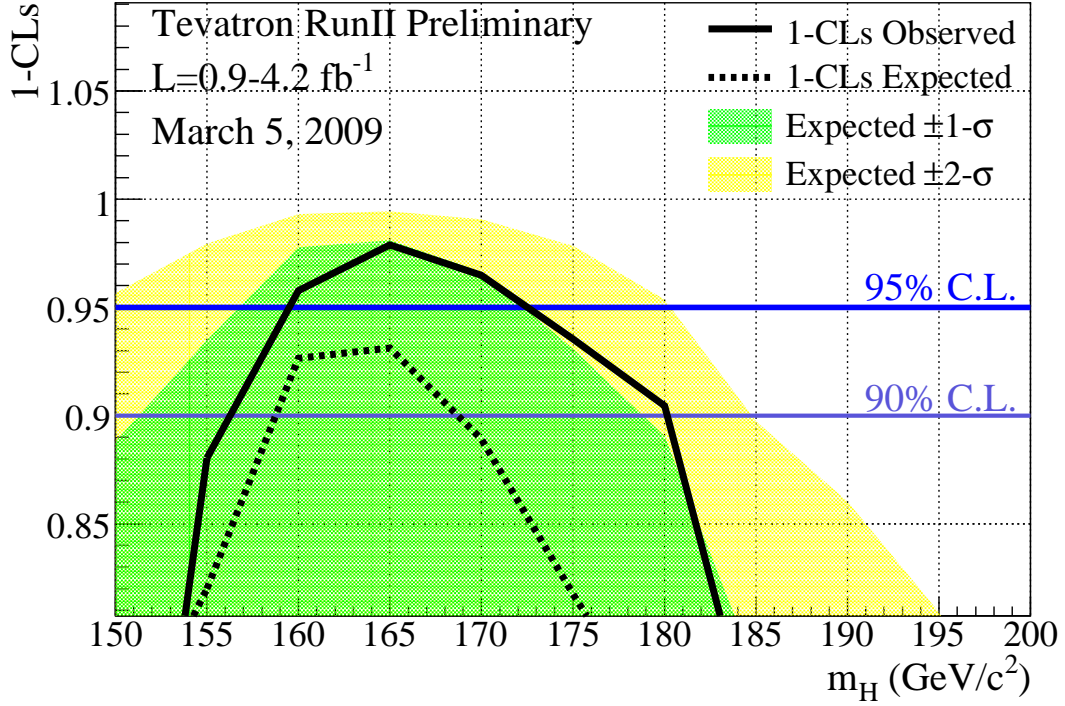


FIG. 5: Distributions of $1-CL_S$ as a function of the Higgs boson mass (in steps of $5 \text{ GeV}/c^2$), as obtained with CL_S method, for the combination of the CDF and DØ analyses.

TABLE XX: Log-likelihood ratio (LLR) values for the combined CDF + DØ Higgs boson search obtained using the CL_S method.

m_H (GeV/c^2)	LLR_{obs}	LLR_{S+B}	$LLR_B^{-2sigma}$	$LLR_B^{-1sigma}$	LLR_B	$LLR_B^{+1sigma}$	$LLR_B^{+2sigma}$
100	2.26	-1.49	5.27	3.17	1.01	-1.21	-3.53
105	1.72	-1.29	5.29	3.19	1.09	-1.09	-3.43
110	0.35	-0.97	4.49	2.71	0.87	-1.03	-3.07
115	0.26	-0.79	4.21	2.53	0.77	-0.99	-2.89
120	0.11	-0.63	3.63	2.11	0.61	-0.93	-2.57
125	-0.01	-0.55	3.41	1.99	0.55	-0.95	-2.43
130	-1.13	-0.55	3.57	2.03	0.57	-0.99	-2.47
135	0.75	-0.57	3.89	2.29	0.73	-0.89	-2.53
140	-0.29	-0.79	4.33	2.61	0.79	-0.95	-2.67
145	-0.93	-0.91	4.71	2.79	0.91	-0.99	-2.99
150	0.16	-1.19	5.63	3.51	1.35	-0.87	-3.17
155	3.02	-1.97	7.07	4.47	1.85	-0.85	-3.67
160	5.02	-3.51	9.93	6.71	3.39	-0.15	-3.81
165	6.60	-3.81	10.23	6.89	3.49	-0.07	-3.91
170	5.58	-2.83	8.67	5.67	2.65	-0.51	-3.85
175	4.59	-1.89	7.01	4.41	1.87	-0.81	-3.63
180	3.95	-1.41	5.75	3.63	1.41	-0.89	-3.39
185	2.04	-0.77	4.09	2.43	0.75	-0.97	-2.79
190	2.04	-0.51	3.33	1.95	0.55	-0.89	-2.45
195	1.19	-0.37	2.75	1.57	0.39	-0.85	-2.11
200	0.80	-0.29	2.41	1.37	0.31	-0.79	-1.93

-
- [1] CDF Collaboration, “Combined Upper Limit on Standard Model Higgs Boson Production for Winter 2009”, CDF Conference Note 9674 (2009).
- [2] DØ Collaboration, “Combined upper limits on standard model Higgs boson production from the DØ experiment with up to 4.2 fb⁻¹ of data” DØ Conference Note 5896 (2009).
- [3] CDF Collaboration, “Combined Upper Limit on Standard Model Higgs Boson Production for Summer 2008”, CDF Conference Note 9502 (2008).
- [4] DØ Collaboration, “Combined upper limits on standard model Higgs boson production from the DØ experiment in 1.1-3.0 fb⁻¹” DØ Conference Note 5756 (2008).
- [5] The CDF and DØ Collaborations and the TEVNPHWG Working Group, “Combined CDF and DØ Upper Limits on Standard Model Higgs Boson Production at Higg Mass (155-200 GeV) with 3 fb⁻¹ of Data”, FERMILAB-PUB-08-270-E, CDF Note 9465, DØ Note 5754, arXiv:0808.0534v1 [hep-ex] (2008).
- [6] The CDF and DØ Collaborations and the TEVNPHWG Working Group, “Combined CDF and DØ Upper Limits on Standard Model Higgs Boson Production with up to 2.4 fb⁻¹ of Data”, FERMILAB-PUB-08-069-E, CDF Note 9290, DØ Note 5645, arXiv:0804.3423v1 [hep-ex] (2008).
- [7] CDF Collaboration, “Search for Higgs Boson Production in Association with W^\pm Boson with 2.7 fb⁻¹”, CDF Conference Note 9468 (2008);
CDF Collaboration, “Search for Standard Model Higgs Boson Production in Association with a W Boson Using Matrix Element and Boosted Decision Tree Techniques with 2.7 fb⁻¹ of Data”, CDF Conference Note 9463 (2008);
CDF Collaboration, “Combined $WH \rightarrow \ell\nu b\bar{b}$ search with 2.7 fb⁻¹ of CDF data”, CDF Conference Note 9596 (2008).
- [8] CDF Collaboration, “Search for the Standard Model Higgs Boson in the \cancel{E}_T Plus Jets Sample”, CDF Conference Note 9642 (2008).
- [9] CDF Collaboration, “A Search for $ZH \rightarrow \ell^+\ell^-b\bar{b}$ in 2.7 fb⁻¹ using a Neural Network Discriminant”, CDF Conference Note 9665 (2009).
- [10] CDF Collaboration, “Search for $H \rightarrow WW^*$ Production Using 3.6 fb⁻¹ of Data”, CDF Conference Note 9500 (2009).
- [11] CDF Collaboration, “Search for SM Higgs using tau leptons using 2 fb⁻¹”, CDF Conference Note 9179.
- [12] CDF Collaboration, “A Search for the Standard Model Higgs Boson in the All-Hadronic channel using a Matrix Element Method”, CDF Conference Note 9366.
- [13] DØ Collaboration, “Search for WH associated production using a combined Neural Network and Matrix Element approach with 2.7 fb⁻¹ of Run II data,” DØ Conference Note 5828.
- [14] DØ Collaboration, “Search for the standard model Higgs boson in τ final states”, DØ Conference note 5883.
- [15] DØ Collaboration, “Search for the standard model Higgs boson in the $HZ \rightarrow b\bar{b}\nu\nu$ channel in 2.1 fb⁻¹ of $p\bar{p}$ collisions at $\sqrt{s} = 1.96$ TeV”, DØ Conference note 5586.
- [16] DØ Collaboration, “A Search for $ZH \rightarrow \ell^+\ell^-b\bar{b}$ Production at DØ in $p\bar{p}$ Collisions at $\sqrt{s} = 1.96$ TeV”, DØ Conference Note 5570.
- [17] DØ Collaboration, “Search for associated Higgs boson production $WH \rightarrow WWW^* \rightarrow \ell^\pm\nu\ell'^\pm\nu' + X$ in $p\bar{p}$ collisions at $\sqrt{s} = 1.96$ TeV”, DØ Conference Note 5485.
- [18] DØ Collaboration, “Search for Higgs production in dilepton plus missing energy final states with 3.0–4.2 fb⁻¹ of $p\bar{p}$ collisions at $\sqrt{s} = 1.96$ TeV”, DØ Conference Note 5871.
- [19] DØ Collaboration, “Search for the Standard Model Higgs boson in $\gamma\gamma$ final state with 4.2 fb⁻¹ data”, DØ Conference Note 5858.
- [20] DØ Collaboration, “Search for the standard model Higgs boson in the $t\bar{t}H \rightarrow t\bar{t}b\bar{b}$ channel”, DØ Conference note 5739.
- [21] K. O. Stanley and R. Miikkulainen, “Evolutionary Computation”, **10 (2)** 99-127 (2002);
S. Whiteson and D. Whiteson, hep-ex/0607012 (2006).
- [22] T. Sjöstrand, L. Lonnblad and S. Mrenna, “PYTHIA 6.2: Physics and manual,” arXiv:hep-ph/0108264.
- [23] H. L. Lai *et al.*, “Improved Parton Distributions from Global Analysis of Recent Deep Inelastic Scattering and Inclusive Jet Data”, Phys. Rev D **55**, 1280 (1997).
- [24] C. Anastasiou, R. Boughezal and F. Petriello, “Mixed QCD-electroweak corrections to Higgs boson production in gluon fusion”, arXiv:0811.3458 [hep-ph] (2008).
- [25] D. de Florian and M. Grazzini, “Higgs production through gluon fusion: updated cross sections at the Tevatron and the LHC”, arXiv:0901.2427v1 [hep-ph] (2009).
- [26] S. Catani, D. de Florian, M. Grazzini and P. Nason, “Soft-gluon resummation for Higgs boson production at hadron colliders,” JHEP **0307**, 028 (2003) [arXiv:hep-ph/0306211].
- [27] K. A. Assamagan *et al.* [Higgs Working Group Collaboration], “The Higgs working group: Summary report 2003,” arXiv:hep-ph/0406152.

- [28] U. Aglietti, R. Bonciani, G. Degrossi, A. Vicini, “Two-loop electroweak corrections to Higgs production in proton-proton collisions”, arXiv:hep-ph/0610033v1 (2006).
- [29] A. D. Martin, W. J. Stirling, R. S. Thorne and G. Watt, “Parton distributions for the LHC”, arXiv:0901.0002 [hep-ph] (2009).
- [30] A. D. Martin, R. G. Roberts, W. J. Stirling and R. S. Thorne, Phys. Lett. B **531**, 216 (2002) [arXiv:hep-ph/0201127].
- [31] O. Brein, A. Djouadi, and R. Harlander, “NNLO QCD corrections to the Higgs-strahlung processes at hadron colliders”, Phys. Lett. B579, 2004, 149-156.
- [32] Ciccolini, M. L. and Dittmaier, S. and Kramer, M., “Electroweak radiative corrections to associated W H and Z H production at hadron colliders”, Phys. Rev. D68 (2003) 073003.
- [33] E. Berger and J. Campbell. “Higgs boson production in weak boson fusion at next-to-leading order”, Phys. Rev. D70 (2004) 073011,
- [34] A. Djouadi, J. Kalinowski and M. Spira, “HDECAY: A program for Higgs boson decays in the standard model and its supersymmetric extension,” Comput. Phys. Commun. **108**, 56 (1998) [arXiv:hep-ph/9704448].
- [35] M. L. Mangano, M. Moretti, F. Piccinini, R. Pittau and A. D. Polosa, “ALPGEN, a generator for hard multiparton processes in hadronic collisions,” JHEP **0307**, 001 (2003) [arXiv:hep-ph/0206293].
- [36] S. Frixione and B.R. Webber, JHEP 06, 029 (2002) [arXiv:hep-ph/0204244]
- [37] G. Corcella *et al.*, “HERWIG 6: An event generator for hadron emission reactions with interfering gluons (including supersymmetric processes),” JHEP **0101**, 010 (2001) [arXiv:hep-ph/0011363].
- [38] A. Pukhov *et al.*, “CompHEP: A package for evaluation of Feynman diagrams and integration over multi-particle phase space. User’s manual for version 33,” [arXiv:hep-ph/9908288].
- [39] J. Campbell and R. K. Ellis, <http://mcfm.fnal.gov/>.
- [40] T. Junk, Nucl. Instrum. Meth. A434, p. 435-443, 1999, A.L. Read, “Modified frequentist analysis of search results (the CL_s method)”, in F. James, L. Lyons and Y. Perrin (eds.), *Workshop on Confidence Limits*, CERN, Yellow Report 2000-005, available through cdsweb.cern.ch.
- [41] W. Fisher, “Systematics and Limit Calculations,” FERMILAB-TM-2386-E.